

# A SPECTROSCOPIC STUDY OF NUCLEAR PROCESSING AND PRODUCTION OF ANOMALOUSLY STRONG LINES IN THE CRAB NEBULA <sup>1</sup>

Gordon M. MacAlpine, Tait C. Ecklund, William R. Lester, Steven J. Vanderveer

*Department of Physics and Astronomy, Trinity University, San Antonio, TX 78212*

and

Louis-Gregory Strolger

*Department of Physics and Astronomy, Western Kentucky University, Bowling Green, KY  
42101*

## ABSTRACT

We present and discuss correlations for optical and near-infrared (5500 – 10030 Å) line intensity measurements at many positions in the Crab Nebula. These correlations suggest the existence of gas produced by a range of nuclear processing, from material in which synthesis ended with the CNO-cycle, to some helium-burning and nitrogen depletion, to regions containing enriched products of oxygen-burning. The latter exhibit a gradual, linear rise of [Ni II] emission with increasing argon enrichment, whereas gas with less nuclear processing shows markedly different [Ni II] emission characteristics, including the highest derived abundances. This suggests two origins for stable, neutron-rich nickel in the nebula: a type of “alpha-rich freezeout” in the more highly processed material, and possibly removal of ions from the neutron star in other regions. In addition, the data indicate that anomalously strong observed [C I] emission comes from broad, low-ionization H<sup>+</sup> to H<sup>0</sup> transition zones. Although the strongest He I emission could also be enhanced in similar low-ionization gas, correlations between relevant line ratios argue against that interpretation, strengthening the case for an exceptionally high helium mass fraction in some locations.

*Subject headings:* ISM: individual (Crab Nebula)—nuclear reactions, nucleosynthesis, abundances — pulsars: individual (PSR 0531 +21) — stars: neutron—supernovae: individual (SN 1054) — supernova remnants

---

<sup>1</sup>This paper involves data obtained at the Michigan-Dartmouth-MIT Observatory and at the McDonald Observatory of The University of Texas at Austin.

## 1. INTRODUCTION

Young supernova remnants are excellent laboratories for investigating how stars make elements, and the Crab Nebula in particular can provide unique information about the precursor star, the supernova event, associated heavy element production, and the environment of a highly energetic pulsar. It is the bright remnant of a core-collapse supernova observed in 1054 A.D. Its age and location, roughly 180 pc away from the plane of the Galaxy, suggest that the ejecta are not significantly contaminated by swept-up interstellar material. Furthermore, measured electron temperatures in the gas (Woltjer 1958; Miller 1978; Fesen & Kirshner 1982; MacAlpine et al. 1989, 1996) along with the lack of other possible evidence for shocks (Frail et al. 1995) imply that the line-emitting gas shines primarily because of photoionization by the locally-generated synchrotron radiation field (see also Davidson & Fesen 1985). Therefore it can be analyzed using powerful numerical photoionization modeling codes. It is generally believed that the supernova precursor star initially contained about  $9 - 11 M_{\odot}$  (e.g., Arnett 1975; Nomoto 1985), representing the important low end of the Type II supernova mass range, below which stars could ignite carbon degenerately and above which successive nuclear reaction stages would be expected to take place through silicon burning. As discussed by Woosley & Weaver (1986a), the applicable stellar models allow for a number of explosive and nucleosynthesis possibilities.

Spectroscopic and photometric investigations of the Crab Nebula to date have indicated several apparent “gas components.” The majority of the observed nebular gas is helium (e.g., MacAlpine et al. 1989), consisting of less than  $2 M_{\odot}$  (MacAlpine & Uomoto 1991). It has been postulated that this represents “helium mantle” material from deep within the original star, ejected by the explosive event. This is consistent with some stellar models, or scenarios involving another star, in which outer layers of the precursor were lost prior to the core-collapse event. Most of this helium-mantle gas appears to be nitrogen-rich, confirming its origin from CNO processing (MacAlpine et al. 1996).

There also is a major component of gas, primarily in the southern part of the nebula near the pulsar, which is significantly nitrogen-poor and much of which is sulfur-rich (MacAlpine et al. 1996). It was suggested that this gas resulted from localized oxygen-burning episodes, consistent with stellar models (Woosley & Weaver 1986b, 1995) that involve off-center (in a shell) oxygen-burning. Strolger & MacAlpine (1996) provided a preliminary demonstration that this explanation is probably correct.

Still another significant nebular component or “anomaly” involves an apparent helium-rich torus viewed as an east-west band across the pulsar region, which constitutes approximately 25% of the visible material (Uomoto & MacAlpine 1987; MacAlpine et al. 1989; MacAlpine & Uomoto 1991). The computed helium mass fraction is about 95%, and there

is not yet a realistic explanation for this apparent structure.

Other known apparent anomalies in the Crab Nebula include exceptionally strong [Ni II] and [C I] line emission, resulting in large spatial variations for deduced abundances of nickel (along with iron) and carbon. Strong [Ni II]  $\lambda 7378$  has been reported by numerous authors (Miller 1978; Fesen & Kirshner 1982; Henry et al. 1984; MacAlpine et al. 1989). The latter work suggested neutron-rich nickel isotopic abundance enhancements, compared with solar, by factors of 5-50 at various locations. Iron was also found to vary widely, together with nickel but at a much lower level; deduced nickel/iron abundance ratios are roughly 60-75 times the solar value.

Henry et al. (1984) found surprisingly high [C I]  $\lambda\lambda 9823, 9850$  emission at several locations in the Crab Nebula, where it was measured to be as much as 7 times stronger than predicted by the photoionization models of Henry & MacAlpine (1982). To account for this, it was postulated that the [C I] lines might arise from collisional excitation involving hydrogen atoms as well as electrons.

As part of an effort to develop a more consistent and accurate overall understanding of the Crab Nebula, we have measured relative line intensities of He I  $\lambda 5876$ , [O I]  $\lambda 6300$ ,  $H\alpha$ , [N II]  $\lambda 6583$ , [Ar III]  $\lambda 7136$ , [Ni II]  $\lambda 7378$ , [S III]  $\lambda 9069$ , [S III]  $\lambda 9531$ , and [C I]  $\lambda 9850$  for roughly 200 well-distributed positions throughout the emitting gas. In this paper, we address all of the above issues (apparent gas components and anomalies) using comparisons among these line measurements. A follow-up paper, involving more in-depth photoionization analyses for deriving improved gas physical conditions and chemical abundances, is planned.

The spectroscopic observations are described in § 2. Then § 3 presents emission-line correlations and resulting inferences about the nebular gas. The correlations illustrate a broad range of nuclear processing and confirm significant enrichment with products of oxygen-burning in some areas. They also suggest two distinct nickel/argon line relationships. In addition, the importance of optical depth for enhanced [C I] lines is demonstrated, along with the *lack* of a dominant role for optical depth in the production of strong He I emission. A summary discussion is given in § 4.

## 2. OBSERVATIONS

Spectroscopy covering the wavelength range from approximately 5500 to 7700 Å was obtained through a long slit at various orientations across the pulsar during the nights of 1995 January 21 and 22, at the 2.4-m Hiltner telescope of the former Michigan-Dartmouth-MIT Observatory, which is located on Kitt Peak. The Mark III spectrograph was used with

a TEK 1024×1024 CCD and a 600 lines mm<sup>-1</sup> grism blazed at 5800 Å, resulting in roughly 2.3 Å pixel<sup>-1</sup> dispersion. The slit width was 1''2, projected on the sky, and the effective projected length was about 4'5. The slit positions employed for this project are illustrated in Figure 1. Each involves alignment through the pulsar and another star, and they are the same as some of the slit orientations used by MacAlpine et al. (1996), in which extensive N-rich and N-poor gas components were first identified. However, the spectral coverage extends further to the red for the optical observations presented here.

Near-infrared spectral coverage (from 7270 to 10030 Å) was obtained during the nights of 2006 January 4 and 5, at the 2.7-m Harlan J. Smith telescope of the McDonald Observatory. The Large Cassegrain Spectrograph was used with the CC1 1024×1024 CCD, grating No. 42, and an RG610 blocking filter. The dispersion through a 2''-wide slit was about 2.7 Å pixel<sup>-1</sup>. The approximately 2'6-long slit was placed in the positions shown with darker outlines in Figure 1 (with overlapping coverage to increase the length in the roughly north-south direction).

Observing conditions on all nights listed above were clear, and exposure times were at least 1 hour at every slit position. All of the optical and near-infrared two-dimensional images were carefully aligned along pixel columns or rows, and the data were reduced to relative flux against linear wavelength using IRAF<sup>2</sup> software, along with observations of both lamp and moonlit-sky continua, wavelength calibration lamps, and spectrophotometric standard stars. Sky spectral observations near the nebula were employed for removing night sky emission from the nebular spectra.

The goal was to identify and extract useful one-dimensional spectra at many positions spatially along the slits. Resulting measured line intensities were corrected for differential dust extinction of  $E(B-V) = 0.47$  (see Davidson & Fesen 1985 and references therein) using the average interstellar extinction table from Osterbrock (1989).

To obtain one-dimensional optical spectra, the dispersed radiation for every spatial pixel along the slits was carefully examined and compared with the associated two-dimensional image. Emission knots were identified, and appropriate combinations of two or three spatial pixels were averaged and extracted for our measurements. In all cases, the individual spectral fluxes for averaged spatial pixels were required to be comparable (within 25% of each other), and no single spatial pixels were used (in order to minimize the possibility of compromising the data by imperfect dispersion pixel alignment). Whereas preliminary measurements were made by more than one person, all of the data employed here were ultimately, consistently

---

<sup>2</sup>The Image Reduction and Analysis Facility (IRAF) is distributed by the Association of Universities for Research in Astronomy, Inc., under contract to the National Science Foundation.

measured by the first author.

A sample optical spectrum is presented in Figure 2. This location was selected for illustration because it has relatively strong [O I], [Ar III], and [Ni II] lines. Two emission systems (e.g., from filaments at the front and back of the expanding nebula) are often represented in the spectra; and here a lower-intensity, near-side system with very weak [N II] emission can also be seen. Sometimes there is line blending, particularly in the wavelength range with [N II]  $\lambda 6548$ ,  $H\alpha$ , and [N II]  $\lambda 6583$ . For such cases, IRAF deblending routines were employed, and occasionally the knowledge that [N II]  $\lambda 6583 \approx 3$  [N II]  $\lambda 6548$  was used in estimating line fluxes. In general, repeated measurements of line fluxes were within 5% of each other. Continuum placement in the optical spectra was reasonably straightforward, and the principal source of error was line blending. Experiments showed that using various reasonable combinations of two or three spatial pixels at a filament location could lead to measurement differences up to 25%, but these changes were always aligned along, or consistent with, the trends to be illustrated and discussed in § 3; so specific pixel selection (following established guidelines) should not alter the conclusions. Actual measurement errors for  $\lambda < 7500$  Å lines are estimated to be less than  $\pm 10\%$ .

A sample near-infrared spectrum, illustrating strong [Ni II], [S III], and [C I] emission, is presented in Figure 3. Whereas there could have been more than one dynamically different emission system represented, line blending was never as much of a problem as in the  $H\alpha$  and [N II] region. Also, we note that these spectra generally involved larger numbers of averaged pixels than was the case for the optical spectra. Although the sky was clear, there were atmospheric seeing problems when the near-infrared data were obtained. This and the larger slit width resulted in somewhat less resolution. In order to obtain broad wavelength coverage, potentially useful line-emission positions in each two-dimensional, near-infrared spectral image were identified and subsequently located as accurately as possible in the corresponding optical two-dimensional image. Then optimal numbers of pixels were averaged to obtain consistent (for all wavelengths) one-dimensional spectra for these filaments. Because of the different slit widths and the fact that we could not expect exact correspondence between optical and near-infrared pixel groupings, it was necessary to normalize the spectra using the overlapped [Ni II]  $\lambda 7378$  line in both wavelength ranges. Although these normalization corrections could be quite accurate and were always less than a factor of 2, they still provided a significant potential source of error (estimated as much as 25%) when comparing near-infrared and optical line intensities.

Another source of error, for one near-infrared line, is telluric water vapor absorption. A plot of measured and reddening corrected values for [S III]  $\lambda 9069$  against [S III]  $\lambda 9531$  shows a tightly defined linear relation (with a linear correlation coefficient greater than 0.99),

as it should for emission from two transitions that arise from the same upper atomic level. However, the predicted slope is about 2.6 for [S III]  $\lambda 9531$  on the vertical axis, according to the relevant transition probabilities given in the current NIST Atomic Spectra Database, whereas the slope of the line in our data is close to 2.0. This type of situation has been reported before (Vermeij et al. 2002) and is caused by water vapor absorption in the 9531 Å wavelength region. The absorption is clearly seen in our standard star spectra, and it should not significantly affect either the [S III]  $\lambda 9069$  or [C I]  $\lambda 9850$  line measurements. Because of this, in § 3 the well-measured [S III]  $\lambda 9069$  line will be used for examining spectral trends, rather than the stronger [S III]  $\lambda 9531$ .

### 3. TRENDS IN THE DATA

All measured He I  $\lambda 5876$ , [O I]  $\lambda 6300$ , [N II]  $\lambda 6583$ , [S II]  $\lambda 6731$ , [Ar III]  $\lambda 7136$ , [Ni II]  $\lambda 7378$ , [S III]  $\lambda 9069$ , and [C I]  $\lambda 9850$  emission line intensities were reddening corrected and normalized to the  $H\alpha$  line. Then they were plotted against each other in various combinations, as we looked for trends that might provide new insights for understanding the physical conditions and chemical abundances in the Crab Nebula, with the future plan of developing improved photoionization models for the emitting gas.

#### 3.1. The Range of Nuclear Processing and Confirmation of Regions with Enhanced Products of Oxygen Burning

As mentioned in the Introduction, MacAlpine et al. (1996) identified regions in the Crab Nebula with either very strong or very weak [N II] emission (see their Figure 1). These gas regimes appear to be distinct both spatially and dynamically. The [N II]-weak gas often (but not always, as discussed below) shows unusually strong [S II] emission, and it was suggested that the latter probably indicates areas which contain products of oxygen-burning. This would be consistent with some stellar models of Woosley & Weaver (1986b, 1995). MacAlpine et al. then used photoionization model analyses to derive overabundances of nitrogen by factors of 3 to 7 (compared with solar) in [N II]-strong regions and overabundances of Si, S, and Ar (assuming solar nitrogen) by factors of 10 to 20 for some [N II]-weak areas.

Enhanced [S II] emission could also result from low-ionization, warm  $H^+ \rightarrow H^0$  transition zones in the emitting gas (Henry & MacAlpine 1982), wherein  $S^+$  ions are effectively collisionally excited by thermal electrons. Therefore, the hypothesis for oxygen-burning products should be further investigated and convincingly demonstrated before its acceptance. There

are ways for examining this issue with the current data; and the most straightforward involve correlations between nitrogen and sulfur emission, between sulfur emission from different ions, or between emission from different elements expected to be produced together by the oxygen-burning process.

Figure 4 shows [N II]  $\lambda 6583$  plotted against [S II]  $\lambda 6731$ . We note the large and comparable range in intensities on both axes. The nitrogen emission can be quite strong with very weak sulfur intensities, representing gas which has progressed no further than the CNO-cycle. Similarly, the strongest sulfur emission correlates only with weak nitrogen, suggestive of advanced processing through oxygen-burning. It may also be seen that weak nitrogen does not always correspond with strong sulfur emission, implying intermediate regions where some helium-burning has taken place and nitrogen has been converted into neon (see Pequignot & Dennefeld 1983; Nomoto 1985; Henry 1986). Regarding the latter point, infrared neon lines have been observed in the Crab Nebula by Temim et al. (2006). Figure 9 of Temim et al. shows particularly strong [Ne II]  $12.8 \mu\text{m}$  emission in an area roughly  $15''$  SW of the pulsar. One of the slits used in this study crosses over an emitting filament at that location, and averages of our measurements there are [N II]  $\lambda 6583/\text{H}\alpha = 0.43$  and [S II]  $\lambda 6731/\text{H}\alpha = 1.5$ . As may be deduced from our Figure 4, these are low [N II] and modest [S II] values that could be expected for a region where helium-burning and nitrogen depletion (to neon) have occurred, but significant oxygen-burning has not taken place.

The data of Figure 4 illustrate the *range* of nuclear processing, but not necessarily the relative *amounts* of material for the various nucleosynthesis stages. Because of line blending and other factors, not all emitting positions could be measured and represented.

Figure 5 is a plot of [S III]  $\lambda 9069$  versus [S II]  $\lambda 6731$ , which argues that the latter line does not arise predominantly in optically-thick  $\text{H}^+ \rightarrow \text{H}^o$  transition regions. Even with potential problems involving normalization of the near-infrared and optical spectra, there is a reasonably strong correlation, with a linear correlation coefficient of 0.75 for 37 points. Therefore, since these different ionization stages (only one of which might be produced in an extended low-ionization zone) increase together, it would appear that strong sulfur emission observed in the Crab Nebula is mainly a result of enhanced sulfur abundance.

In addition to sulfur, other primary products of oxygen-burning include silicon and argon. Silicon emission is not strong in the optical and near-infrared regions, but [Ar III]  $\lambda 7136$  and  $\lambda 7751$  (weaker) can be measured in our data. Therefore, in Figure 6 we plotted the correlation between [Ar III]  $\lambda 7136$  and [S II]  $\lambda 6731$  for 182 locations from the optical slit spectra. In this case, there is no potential problem with spectral normalization, and the correlation is quite high (linear correlation coefficient of 0.91). This confirms that the argon and sulfur emission must represent abundances with a related origin.

Evidence presented here supports the hypothesis (MacAlpine et al. 1996; Strolger & MacAlpine 1996) that certain regions in the Crab Nebula are heavily enriched with products of oxygen-burning. This has important implications for understanding stellar models, and it will be explicitly considered in our follow-up photoionization model analyses. For instance, as pointed out by Henry (1993), high silicon and sulfur abundances would cause infrared fine-structure lines such as [Si II]  $34.8 \mu\text{m}$  and [S III]  $33.6 \mu\text{m}$  to become more important coolants for the gas, thereby influencing the line spectra in the optical and near-infrared. For lower electron temperature, longer-wavelength collisionally-excited lines such as [S II]  $\lambda\lambda 6716, 6731$  and [N II]  $\lambda\lambda 6548, 6583$  would be enhanced at the expense of shorter wavelength lines like [O II]  $\lambda\lambda 3726, 3729$ . Finally, we note that the above infrared fine-structure [Si II] and [S III] lines were recently observed to have significant intensities at some locations in the Crab Nebula (Temim et al. 2006).

Products of oxygen-burning are not unique to the Crab Nebula. Cassiopeia A, another young, collapse-driven, somewhat more massive supernova remnant also exhibits extensive regions with high concentrations of silicon-group elements like sulfur and argon, in which it is recognized that oxygen-burning has taken place while silicon-burning has been incomplete (Chevalier & Kirshner 1979; Willingale et al. 2002).

### 3.2. [Ni II] $\lambda 7378$ and [Ar III] $\lambda 7136$ Line Trends: Possible Implications for the Origin of Nickel

In order to investigate observed very strong nickel emission in the Crab Nebula, we plotted [Ni II] intensity against every other measured line, and we found a particularly interesting correlation with argon. In Figure 7, all optical data are presented for the [Ni II]  $\lambda 7378$  and [Ar III]  $\lambda 7136$  lines. Points below the diagonal show a linear trend (correlation coefficient of 0.86) involving more highly processed gas, whereas points above the diagonal show the strongest [Ni II] emission and tend to represent regions where less nucleosynthesis has occurred.

To investigate or highlight these apparent correlations further, we considered only data for the very lowest and highest nitrogen emission. Following guidelines similar to those used by MacAlpine et al. (1996), we identified the subset of points with measured [N II]  $\lambda 6583 < 0.55 \text{ H}\alpha$  and [N II]  $\lambda 6583 < [\text{S II}] \lambda 6731$  as being extreme “low-N” locations where advanced nuclear processing has taken place. Similarly those points with [N II]  $\lambda 6583 > 3 \text{ H}\alpha$  and [N II]  $\lambda 6583 > [\text{S II}] \lambda 6731$  were selected as being “high-N,” where nucleosynthesis stopped with the CNO-cycle. Figure 8 illustrates how these data appear in the [Ni II]  $\lambda 7378$  versus [Ar III]  $\lambda 7136$  plane, where filled squares represent high-N and open

squares (with a +) denote low-N. The separation of trends in this plot is remarkable, with the low-N (more highly processed) positions having a linear correlation coefficient of 0.94.

Some points below the diagonal of Figure 7 do not appear in Figure 8, either because they do not have measurable [N II] emission or because it is somewhat higher than the imposed limit for inclusion in Figure 8. We also note that, whereas emission from several pixel groups along one extended filament might conceivably create an almost linear structure of points in a diagram, the measurements for Figures 7 and 8 come from widely separated locations in all of the slits.

The linear correlation between [Ni II] and [Ar III] emission from the most highly processed gas could result from a type of “alpha-rich freezeout” (see Woosley & Weaver 1995; Jordan et al. 2003), whereby silicon-group elements in core-collapse supernovae may be heated by a shock wave and broken down into nucleons and alpha particles. Then, as the gas cools, these particles can reassemble into various stable iron-peak nuclei. Another possibly contributing process has been discussed by Thielemann & Arnett (1985), who wrote: “During O-burning, temperatures favor the photodisintegration of heavy nuclei (produced by the s-process) into Fe-peak nuclei. This is seen for  $^{60}\text{Ni}$  and partially for  $^{62}\text{Ni}$  and  $^{58}\text{Fe}$ , depending on the prior neutron excess  $\eta$ .”

The above explanations would not apply to the steeper correlations in Figures 7 and 8, where [Ni II]  $\lambda 7378$  can be strongest in less-processed gas. This may be an indication that some iron-peak, neutron-rich nuclei were removed from the surface of the neutron star. For pulsars in general, this possibility was investigated by Ruderman & Sutherland (1975), who concluded that extremely strong surface magnetic fields would not permit the release of heavy ions for most pulsars. However, they also stated that the Crab Nebula’s neutron star may be an exception to this rule because of very high surface temperature. In this regard, we note that an extremely high temperature region on this young neutron star may have been detected by Weisskopf et al. (2004). Furthermore, Michel et al. (1991) mapped an extensive north-south relativistic wind for the nebula, in the directions of the highest apparent concentrations of nickel (MacAlpine et al 1989). For line-emitting knots immersed in this wind, the highest [Ni II] emission was measured on the side facing the pulsar in each case (MacAlpine et al. 1994; MacAlpine & Lawrence 1994). As Freiburghaus et al. (1999) have noted, the origins of neutron-rich heavy elements are not yet well understood. If ions can leave the surface of the neutron star in the Crab Nebula, then young pulsars in general could represent sources for some heavy nuclei.

### 3.3. On The Origin of Strong [C I] Emission

Henry et al. (1984) measured the strength of [C I]  $\lambda 9850$  in some filaments to be at least several times stronger than predicted by their photoionization models, and they suggested that previously neglected collisional excitation by  $H^0$  may need to be considered as a potentially important process for production of this emission.

If we can understand where and how the [C I] emission is produced, we may be able to use it for estimating the carbon abundance relative to other elements. This, in turn, could provide additional useful insights into the extent of nuclear processing at various locations. As noted by Nomoto (1985) and Henry (1986), the amounts of carbon and oxygen would be depressed somewhat by CNO processing and then would increase (above solar) as a result of helium-burning. Also, Nomoto pointed out that an improved understanding of the carbon abundance, and therefore the amount of processing in the gas, can lead to a more accurate estimate of the stellar precursor mass. Whereas carbon abundances derived from ultraviolet lines like C IV  $\lambda 1549$  for the Crab Nebula may be significantly influenced by the way in which absorption of He II  $\lambda 304$  photons is considered (Eastman et al. 1985), that complication should not be an issue for the [C I]  $\lambda 9850$  line, since it arises away from the He II-emitting gas.

New insight regarding the production of [C I] emission may be gained from examining its correlation with [O I]. As previously shown in Figure 2, the Crab Nebula contains some locations with particularly strong [O I]  $\lambda 6300$  emission, probably indicating the existence of broad  $H^+ \rightarrow H^0$  transition zones in the gas. The [O I] emission is known to be strengthened in these warm low-ionization regions (which could be expected for photoionization by a relatively flat synchrotron spectrum) because  $O^0$  follows  $H^0$  due to very effective charge exchange interactions.

Figure 9 illustrates the correlation between our measured [C I]  $\lambda 9850$  and [O I]  $\lambda 6300$  intensities. Although the plot is affected by the spectrum normalization procedure for near-infrared and optical wavelengths, the linear correlation coefficient is a significantly high 0.81. Therefore, we conclude that the strong [C I] emission is probably enhanced in extended ionization transition zones, by electron collisional excitation and perhaps also by collisions involving  $H^0$ . However, since the C and O contents of the gas could also have been depleted or increased *together* by the CNO-cycle or helium-burning, additional information is needed.

*Indirect* support for the idea that [C I] emission must be strengthened in low-ionization regions also comes from Figure 10, which shows [C I]  $\lambda 9850$  plotted against [N II]  $\lambda 6583$ . There is a rather large (though not extreme) range of [N II] emission represented, and (except for the one very high point) [C I] looks random over an order of magnitude in

the [N II] intensities. Since the latter may provide a rough representation of the amount of nucleosynthesis that has taken place, as discussed previously, it would appear that the strong measured [C I] emission is not directly correlated with nuclear processing. Clearly the roles of both abundance and ionization structure will be important avenues for exploration in further refinements of photoionization model computations.

### 3.4. Exceptionally Strong He I Emission

The final abundance or line-intensity anomaly to be considered here involves the exceptionally high helium content derived by MacAlpine et al. (1989) for an apparent helium torus around the pulsar (see also Lawrence et al. 1995). Having measured dereddened He I  $\lambda 5876 \gtrsim H\beta$ , the results of photoionization analyses by Henry and MacAlpine (1982) were used to infer a helium mass fraction around 95% in this region.

Henry & MacAlpine (1982) also considered the possibility that He I  $\lambda 5876$  recombination lines could be significantly enhanced relative to hydrogen emission in low-ionization zones. Because the photoionization cross section for He<sup>0</sup> scales roughly with frequency as  $\nu^{-2}$ , whereas that for H<sup>0</sup> scales more like  $\nu^{-3}$ , a high energy synchrotron radiation field can continue to ionize helium significantly beyond where hydrogen starts becoming neutral, thereby producing excess He I recombination emission. This process could be especially important if the ionizing radiation flux is low (see, e.g., Shields 1974). However, Henry & MacAlpine found that photoionization models with relatively high values for the ionizing flux did a much better job of matching the majority of observed line intensities in the Crab Nebula, so they favored very high derived abundance as the most plausible explanation for the strongest helium intensities. Now we have the opportunity to investigate this further.

As with [C I] emission, we examined the relation between He I  $\lambda 5876$  and [O I]  $\lambda 6300$  for our data, as shown in Figure 11. It may be seen that evidence for a meaningful correlation is lacking. Strong He I emission is similarly represented at both high and low [O I] intensities, so it is not enhanced primarily in low-ionization gas. Furthermore, we considered the He I  $\lambda 5876$  correlation with [N II]  $\lambda 6583$  in Figure 12. Again, the strongest He I emission is evident with both high and low [N II] measurements, so it apparently is not directly tied to the overall progress of nuclear processing. We conclude that the most reasonable explanation for the strongest He I lines in the apparent torus around the pulsar is anomalously high abundance, the source of which is still in need of a plausible explanation.

#### 4. SUMMARY

We have measured emission of He I  $\lambda 5876$ , [O I]  $\lambda 6300$ , [N II]  $\lambda 6583$ , [S II]  $\lambda 6731$ , [Ar III]  $\lambda 7136$ , [Ni II]  $\lambda 7378$ , [S III]  $\lambda 9069$ , [S III]  $\lambda 9531$ , and [C I]  $\lambda 9850$  at many locations within the Crab Nebula. The different line intensities (or subsets thereof) were plotted against each other in efforts to investigate correlations and improve our understanding of the range of nuclear processing in the gas, as well as the causes of exceptionally strong emission from [Ni II], [C I], and He I. We identified gas where nucleosynthesis has not progressed significantly beyond the CNO-cycle, gas in which some helium-burning and nitrogen depletion have taken place, and regions where oxygen-burning has occurred. The anomalously strong observed [Ni II] emission may have two sources, in one case resulting from high temperature and subsequent cooling in gas enriched with products of oxygen-burning, while in the other case possibly representing the release of nuclei from the neutron star surface. Line correlations indicate that very strong [C I] emission arises in low-ionization  $H^+ \rightarrow H^o$  transition regions. On the other hand, exceptionally strong He I  $\lambda 5876$  does not show similar evidence of a low-ionization zone origin; and it does not appear to correlate with different levels of nuclear processing as represented by [N II] emission. Therefore, the apparent high-helium torus around the pulsar may be a distinct component of the nebula.

We are grateful for generous financial and logistical support from Trinity University and the endowed Charles A. Zilker Chair position. We also thank the staffs of the Michigan-Dartmouth-MIT Observatory and the McDonald Observatory for providing excellent technical assistance with this research.

#### REFERENCES

- Arnett, W. D. 1975, *ApJ*, 195, 727
- Chevalier, R. A., & Kirshner, R. P. 1979, *ApJ*, 233, 154
- Davidson, K., & Fesen, R. A. 1985, *ARA&A*, 23, 119
- Eastman, R. G., MacAlpine, G. M., Kirshner, R. P., & Henry, R. B. C. 1985, in *The Crab Nebula and Related Supernova Remnants*, ed. M. Kafatos and R. B. C. Henry, (Cambridge: Cambridge University Press), 19
- Fesen, R. A., & Kirshner, R. P. 1982, *ApJ*, 258, 1
- Frail, D. A., Kassim, N. E., Cornwell, T. J., & Goss, W. M. 1995, *ApJ*, 454, L129

- Freiburghaus, C., Rosswog, S., & Thielemann, F-K. 1999, *ApJ*, 525, L121
- Henry, R. B. C. 1986, *PASP*, 98, 1044
- Henry, R. B. C. 1993, *MNRAS*, 261, 306
- Henry, R. B. C., & MacAlpine, G. M. 1982, *ApJ*, 258, 11
- Henry, R. B. C., MacAlpine, G. M., & Kirshner, R. P. 1984, *ApJ*, 278, 619
- Jordan, G. C., Gupta, S. S., & Meyer, B. S. 2003, *Phys. Rev. C*, 68, 065801
- Lawrence, S. S., MacAlpine, G. M., Uomoto, A., Woodgate, B. E., Brown, L. W., Oliverson, R. J., Lowenthal, J. D., & Liu, C. 1995, *AJ*, 109, 2635
- MacAlpine, G. M., & Lawrence, S. S. 1994, in *The Analysis of Emission Lines, Poster Papers from The 8th Space Telescope Science Institute Symposium*, ed. R. E. Williams and M. Livio, StSci Publication
- MacAlpine, G. M., Lawrence, S. S., Brown, B. A., Uomoto, A., Woodgate, B. E., Brown, L. W., Oliverson, R. J., Lowenthal, J. D., & Liu, C. 1994, *ApJ*, 432, L131
- MacAlpine, G. M., Lawrence, S. L., Sears, R. L., Sosin, M. S., & Henry, R. B. C. 1996, *ApJ*, 463, 650
- MacAlpine, G. M., McGaugh, S. S., Mazzarella, J. M., & Uomoto, A. 1989, *ApJ*, 342, 364
- MacAlpine, G. M., & Uomoto, A. 1991, *AJ*, 102, 218
- Michel, F. C., Scowen, P. A., Dufour, R. J., & Hester, J. J. 1991, *ApJ*, 368, 463
- Miller, J. S. 1978, *ApJ*, 220, 490
- NIST Atomic Spectra Database. Version 3.0.3. January 2006. National Institute of Standards and Technology. 10 June 2006 <<http://physics.nist.gov/PhysRefData/ASD/index.html>>
- Nomoto, K. 1985, in *The Crab Nebula and Related Supernova Remnants*, ed. M. Kafatos and R. B. C. Henry (Cambridge: Cambridge University Press), 97
- Osterbrock, D. E. 1989, *Astrophysics of Gaseous Nebulae and Active Galactic Nuclei* (Mill Valley: University Science Books)
- Pequignot, D., & Dennefeld, M. 1983, *Astr. Ap.*, 120, 249

- Ruderman, M. A., & Sutherland, P. G. 1975, *ApJ*, 196, 51
- Shields, G. A. 1974, *ApJ*, 191, 309
- Strolger, L-G., & MacAlpine, G. M. 1996, *BAAS*, vol. 28, 950
- Temim, T., Gehrz, R. D., Woodward, C. E., Roellig, T. L., Smith, N., Rudnick, L. R., Polomski, E. F., Davidson, K., Yuen, L., & Onaka, T. 2006, preprint (astro-ph/0606321)
- Thielemann, F-K., & Arnett, W. D. 1985, in *Nucleosynthesis: Challenges and New Developments*, eds. Arnett, W. D. and Truran, J. W. (Univ. of Chicago Press: Chicago & London), 170
- Uomoto, A., & MacAlpine, G. M. 1987, *AJ*, 93, 1511
- Vermeij, R., Damour, F., van der Hulst, J. M., & Baluteau, J.-P. 2002, *A&A*, 390, 649
- Weisskopf, M. C., O'Dell, S. L., Paerels, F., Elsner, R. F., Becker, W., Tennant, A. F., & Swartz, D. A. 2004, *ApJ*, 601, 1050
- Willingale, R., Bleeker, J. A. M., van der Heyden, K. J., Kaastra, J. S., & Vink, J. 2002, *A&A*, 381, 1039
- Woltjer, L. 1958, *Bull. Astr. Inst. Netherlands*, 14, 39
- Woosley, S. E., & Weaver, T. A. 1986a, *ARA&A*, 24, 205
- Woosley, S. E., & Weaver, T. A. 1986b, in *Nucleosynthesis and Its Implications on Nuclear and Particle Physics*, ed. J. Audouze & N. Mathieu (Dordrecht: Reidel), 145
- Woosley, S. E., & Weaver, T. A. 1995, *APJS*, 101, 181

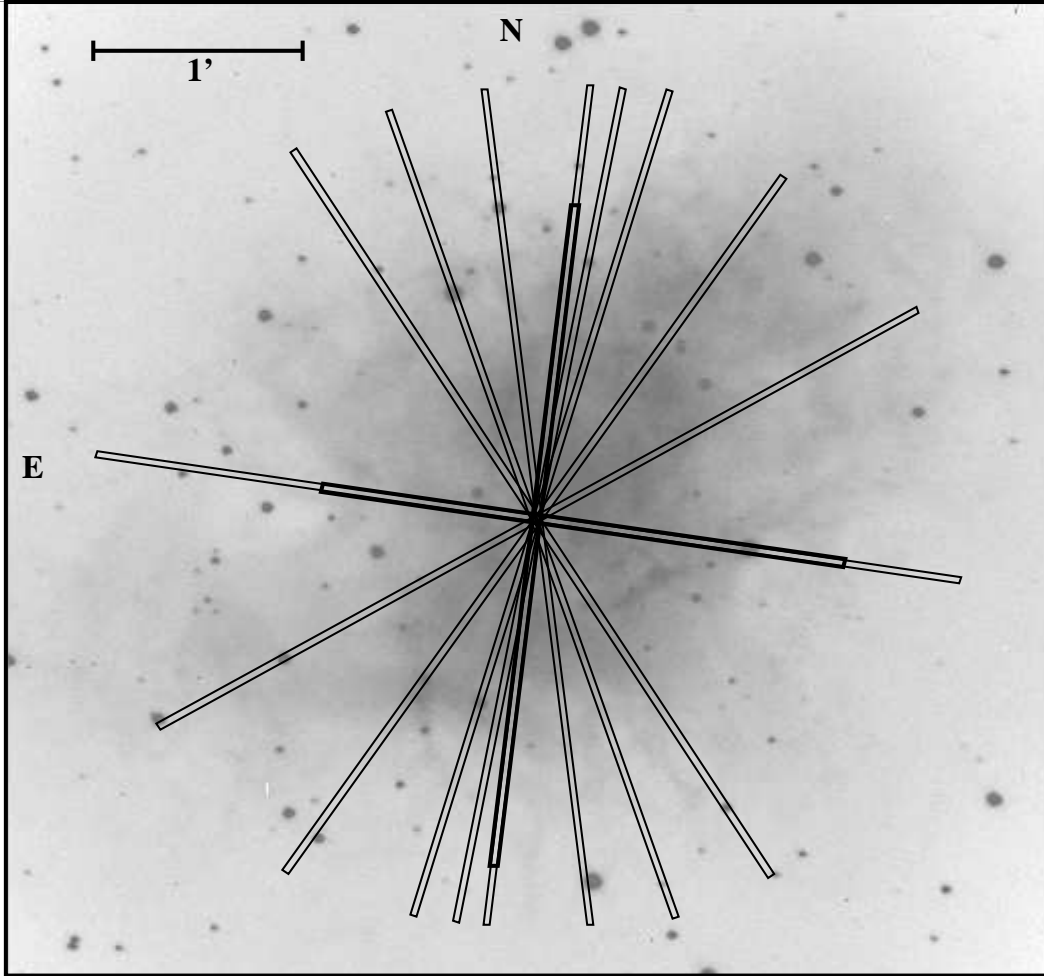


Fig. 1.— Spectroscopic slit locations for this study, superimposed on a V-band image of the Crab Nebula. Each slit crosses over the pulsar and also goes through a separate alignment star. The nearly orthogonal, thicker, shorter slit markers represent locations where near-infrared spectra were obtained.

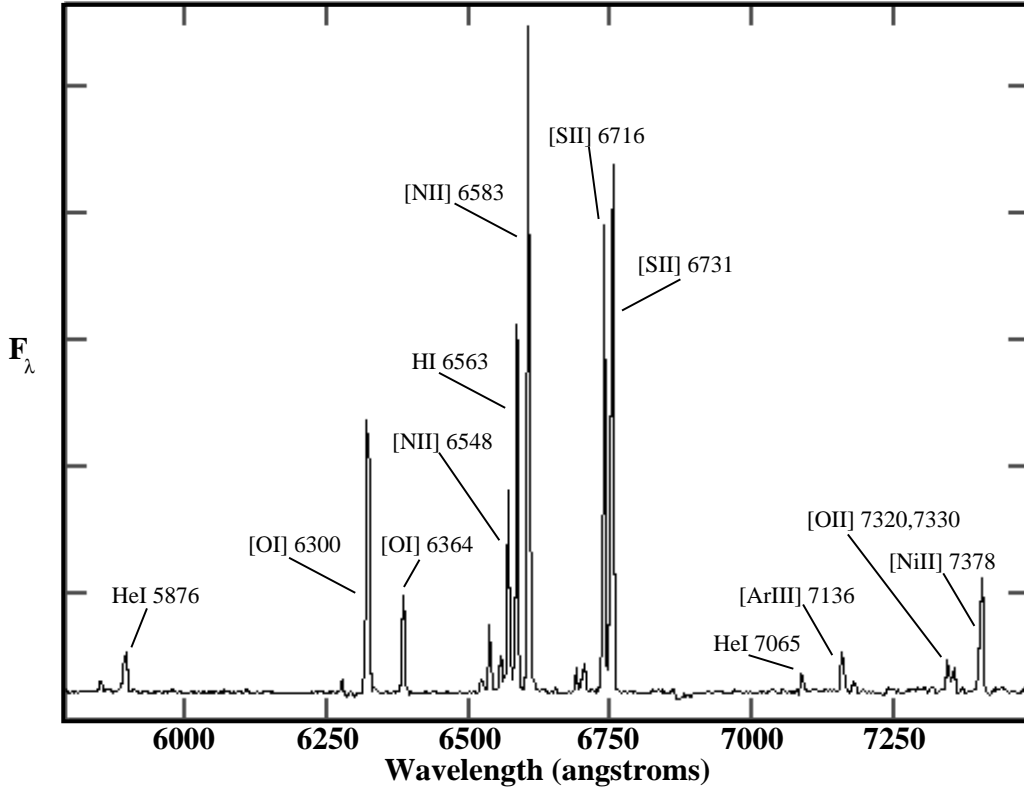


Fig. 2.— A sample optical spectrum, with emission lines identified for gas with  $v \approx +900 \text{ km s}^{-1}$ . Fainter lines for  $v \approx -1200 \text{ km s}^{-1}$  may also be seen. The vertical axis is relative flux density.

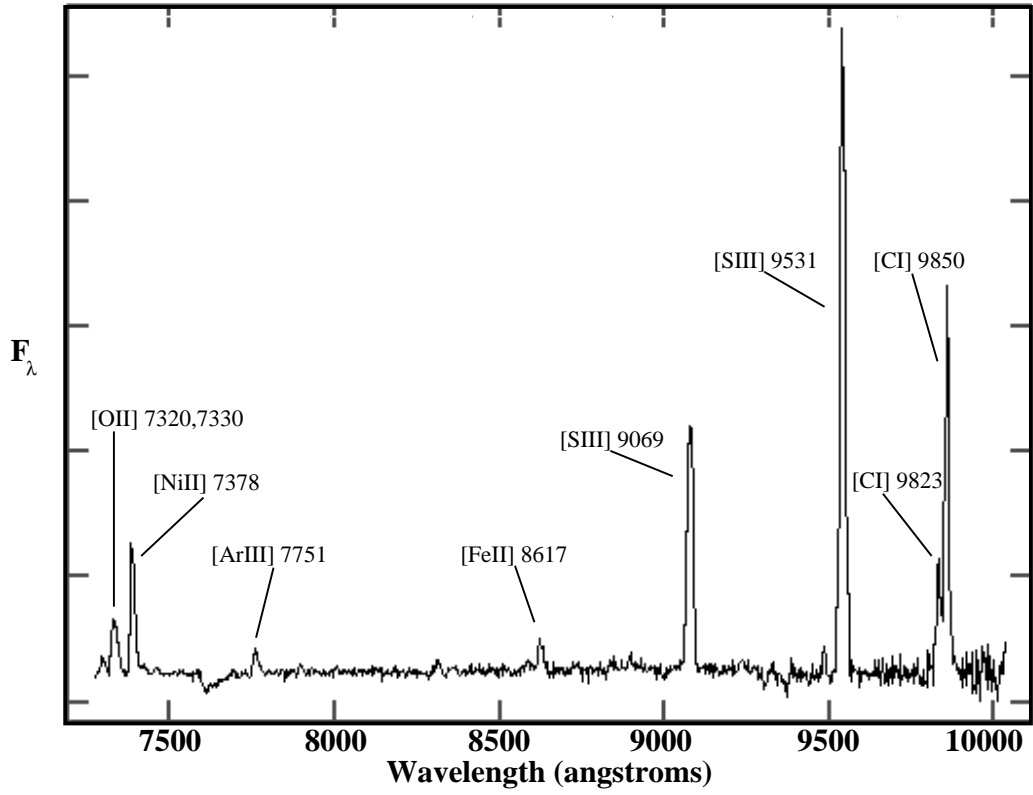


Fig. 3.— A sample near-infrared spectrum with stronger lines indicated. The vertical axis is relative flux density.

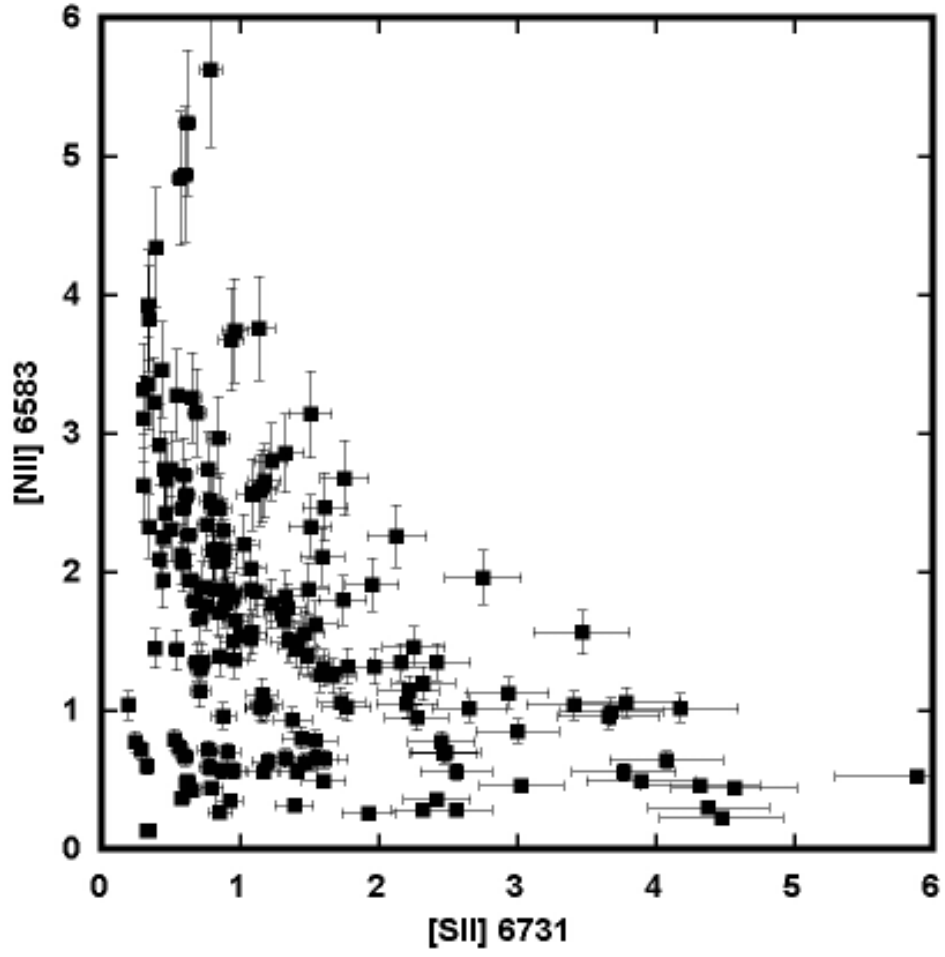


Fig. 4.— Correlation between H $\alpha$ -normalized [N II]  $\lambda$ 6583 and [S II]  $\lambda$ 6731 line intensities. The error bars illustrate  $\pm 10\%$  uncertainties for both axes.

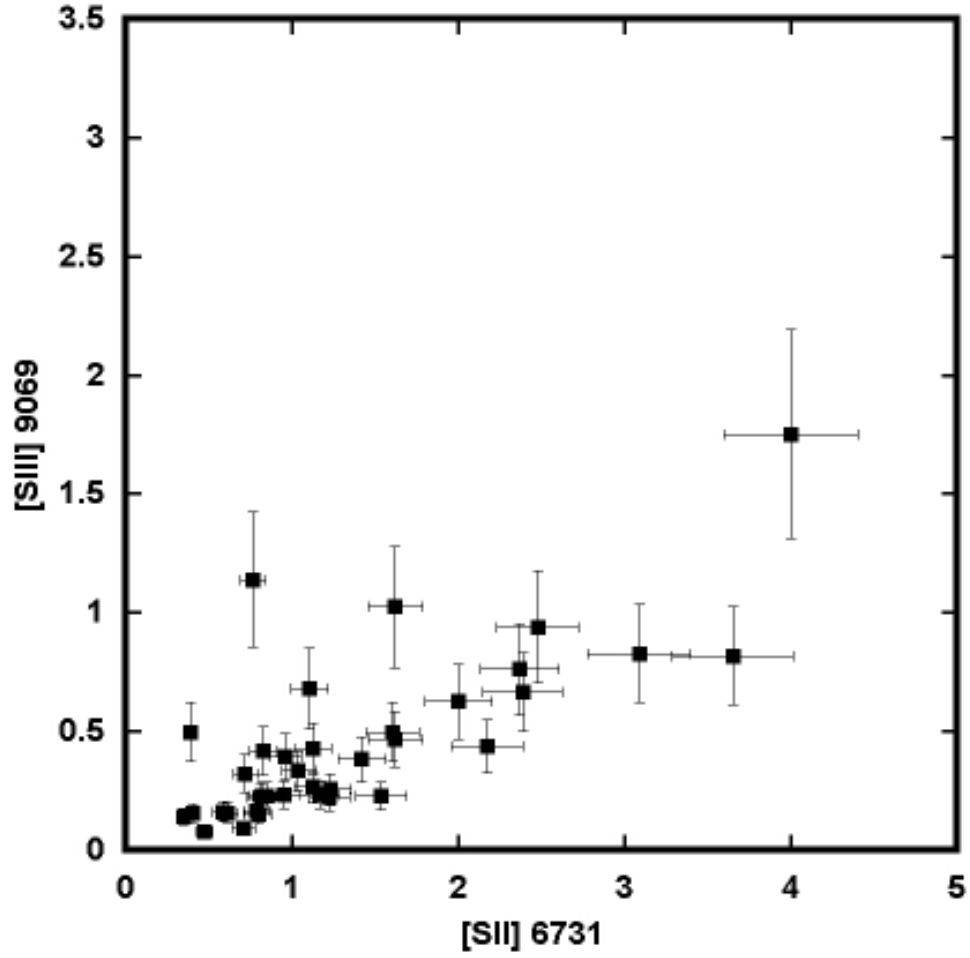


Fig. 5.— Correlation between  $H\alpha$ -normalized  $[S\ III] \lambda 9069$  and  $[S\ II] \lambda 6731$  line intensities for the subset of combined near-infrared and optical measurements. The error bars illustrate uncertainties of  $\pm 10\%$  for  $[S\ II] \lambda 6731$  and  $\pm 25\%$  for  $[S\ III] \lambda 9069$ .

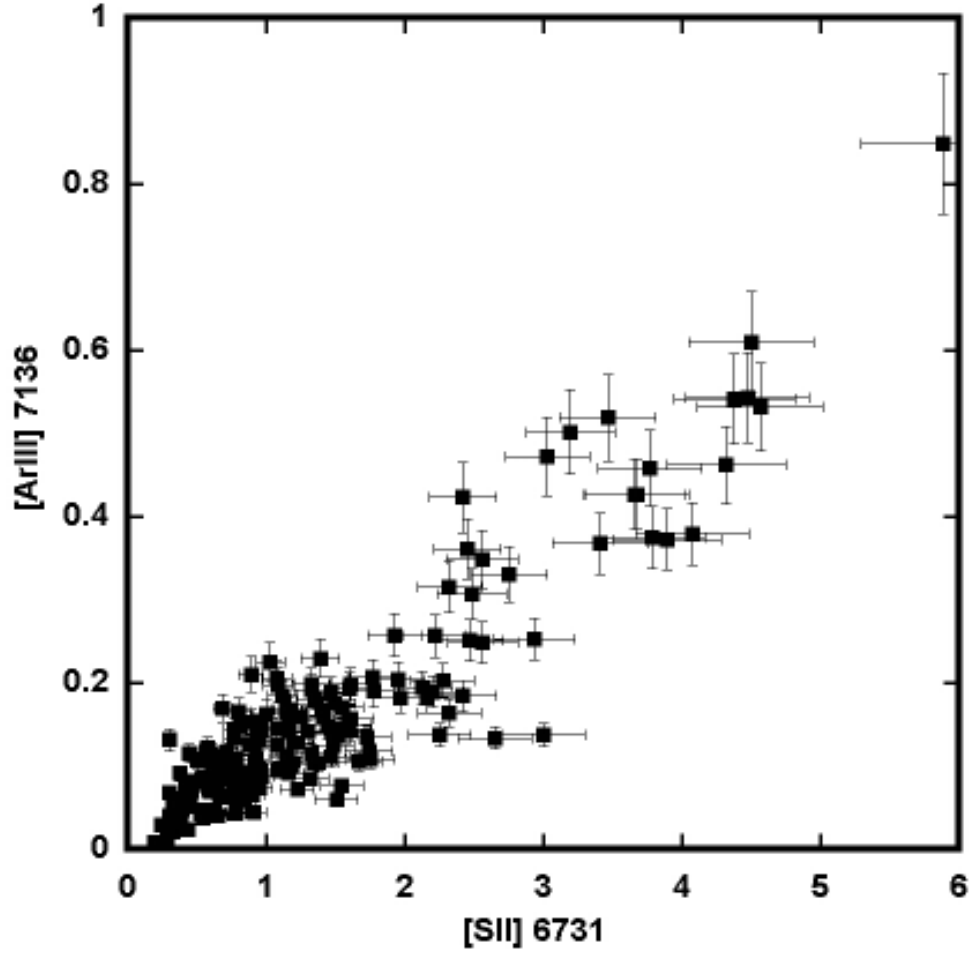


Fig. 6.— Correlation between  $H\alpha$ -normalized  $[\text{Ar III}] \lambda 7136$  and  $[\text{S II}] \lambda 6731$  line intensities. The error bars illustrate  $\pm 10\%$  uncertainties for both axes.

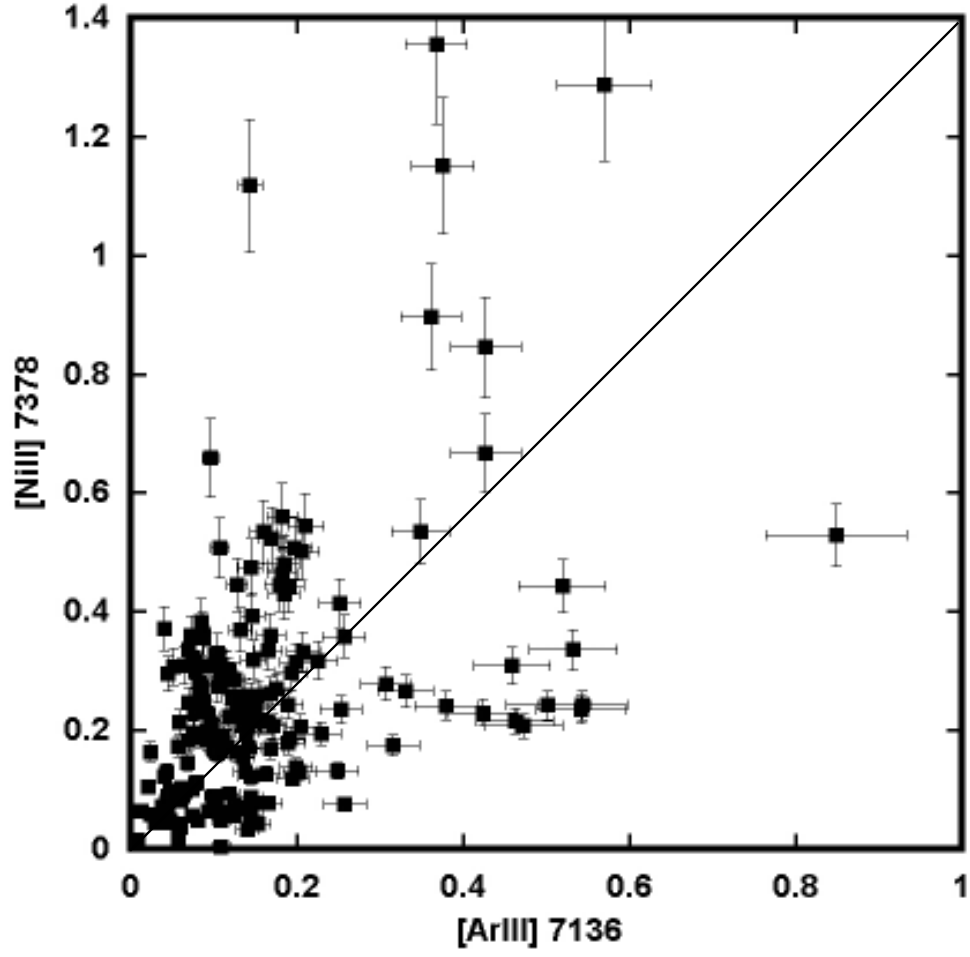


Fig. 7.— Correlation between H $\alpha$ -normalized [Ni II]  $\lambda$ 7378 and [Ar III]  $\lambda$ 7136 line intensities. The error bars illustrate  $\pm 10\%$  uncertainties for both axes.

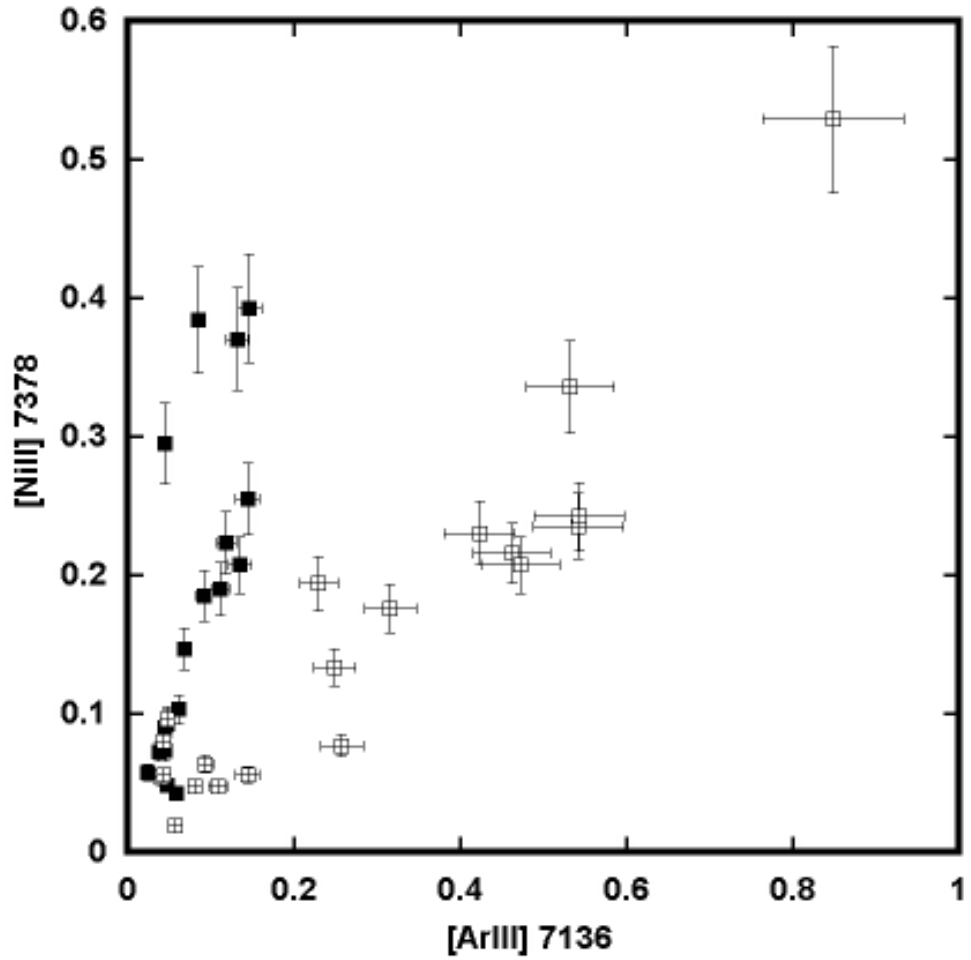


Fig. 8.— Correlation between  $H\alpha$ -normalized  $[\text{Ni II}] \lambda 7378$  and  $[\text{Ar III}] \lambda 7136$  line intensities for the subsets of extreme “high-N” (solid squares) and “low-N” (open squares with +) spectral data, as defined in the text. The error bars illustrate  $\pm 10\%$  uncertainties for both axes.

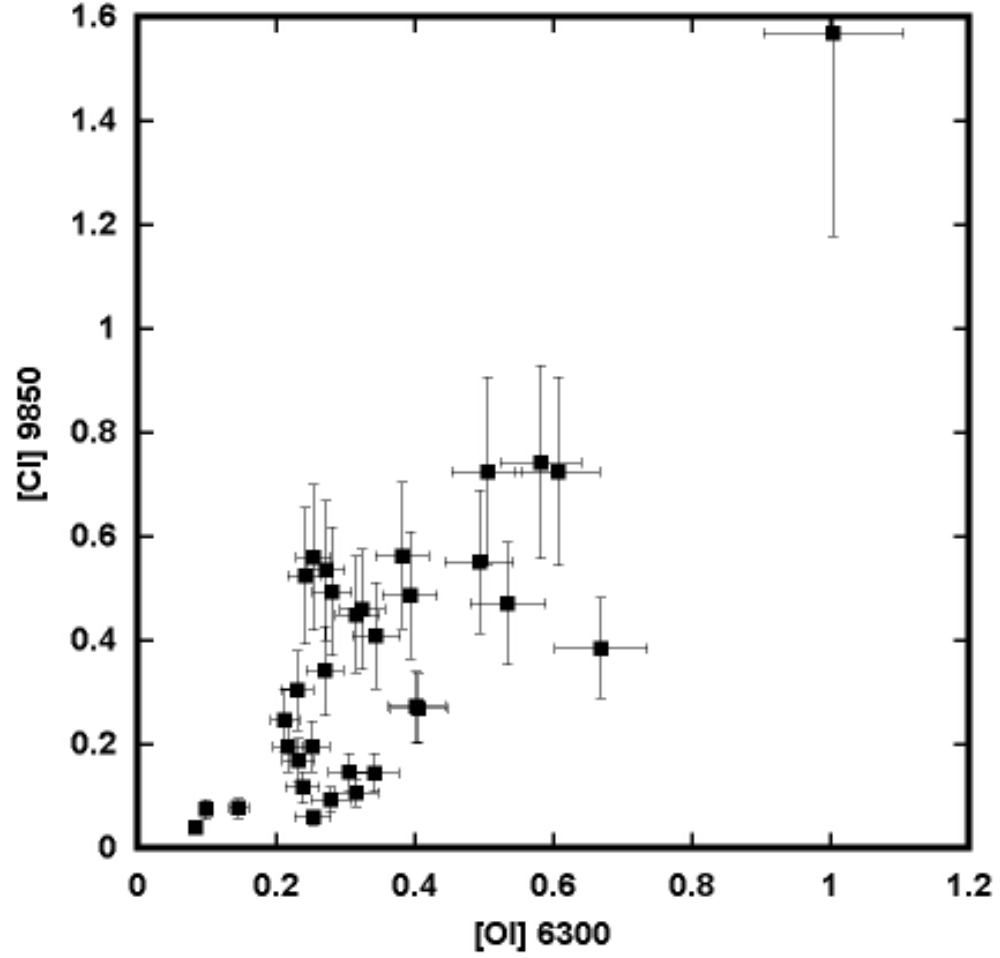


Fig. 9.— Correlation between  $H\alpha$ -normalized [C I]  $\lambda 9850$  and [O I]  $\lambda 6300$  line intensities for the subset of combined near-infrared and optical measurements. The error bars illustrate uncertainties of  $\pm 10\%$  for [O I]  $\lambda 6300$  and  $\pm 25\%$  for [C I]  $\lambda 9850$ .

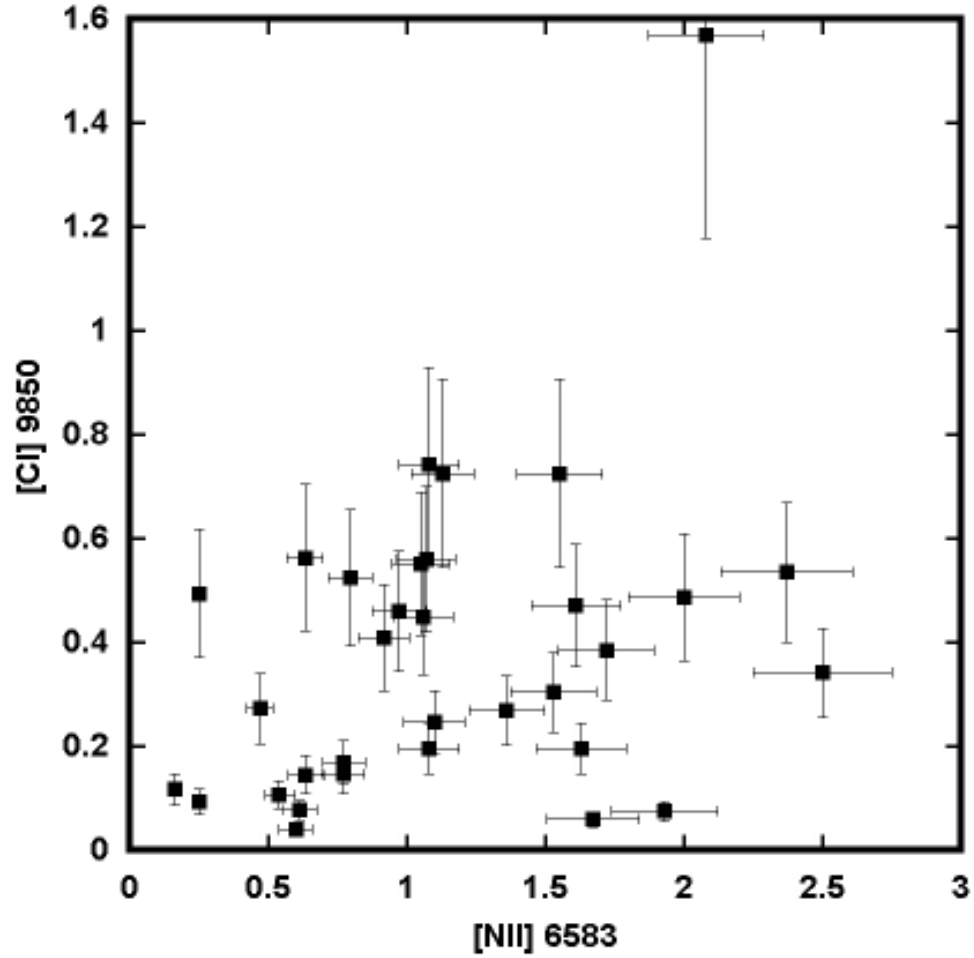


Fig. 10.— Correlation between  $H\alpha$ -normalized  $[C\ I]\ \lambda 9850$  and  $[N\ II]\ \lambda 6583$  line intensities for the subset of combined near-infrared and optical measurements. The error bars illustrate uncertainties of  $\pm 10\%$  for  $[N\ II]\ \lambda 6583$  and  $\pm 25\%$  for  $[C\ I]\ \lambda 9850$ .

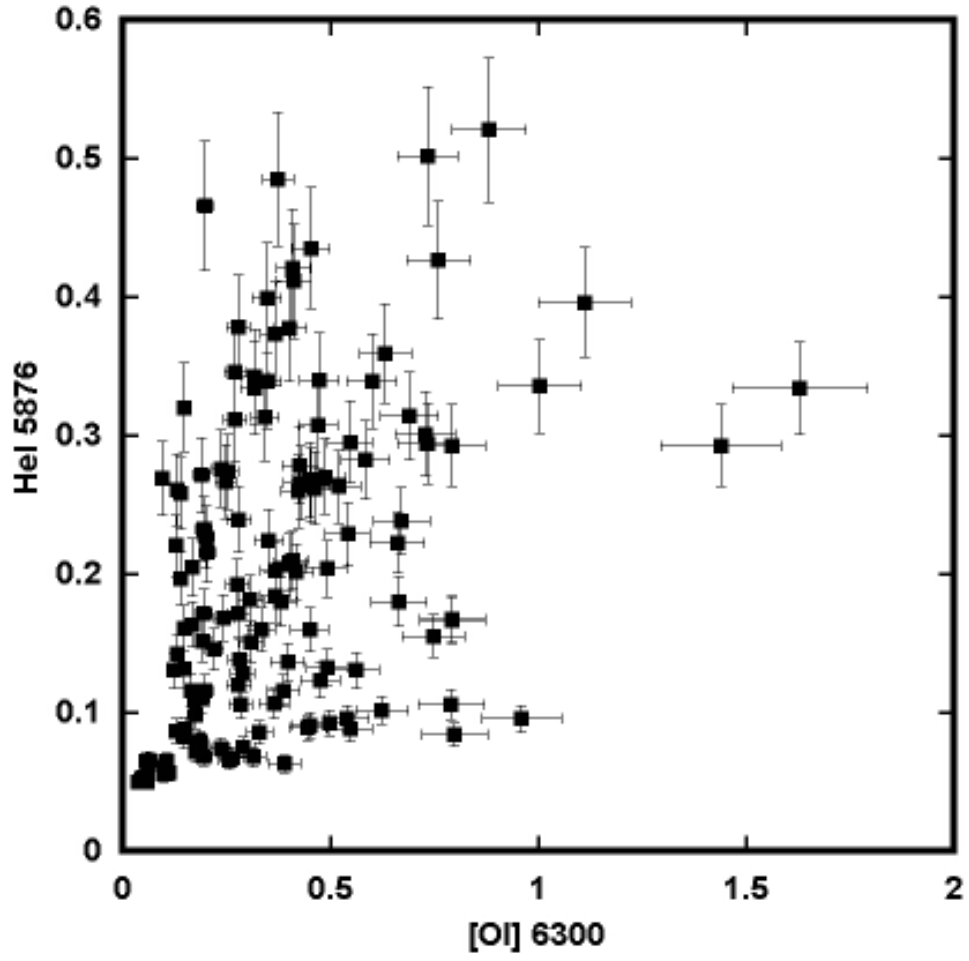


Fig. 11.— Correlation between  $H\alpha$ -normalized He I  $\lambda 5876$  and [O I]  $\lambda 6300$  line intensities. The error bars illustrate  $\pm 10\%$  uncertainties for both axes.

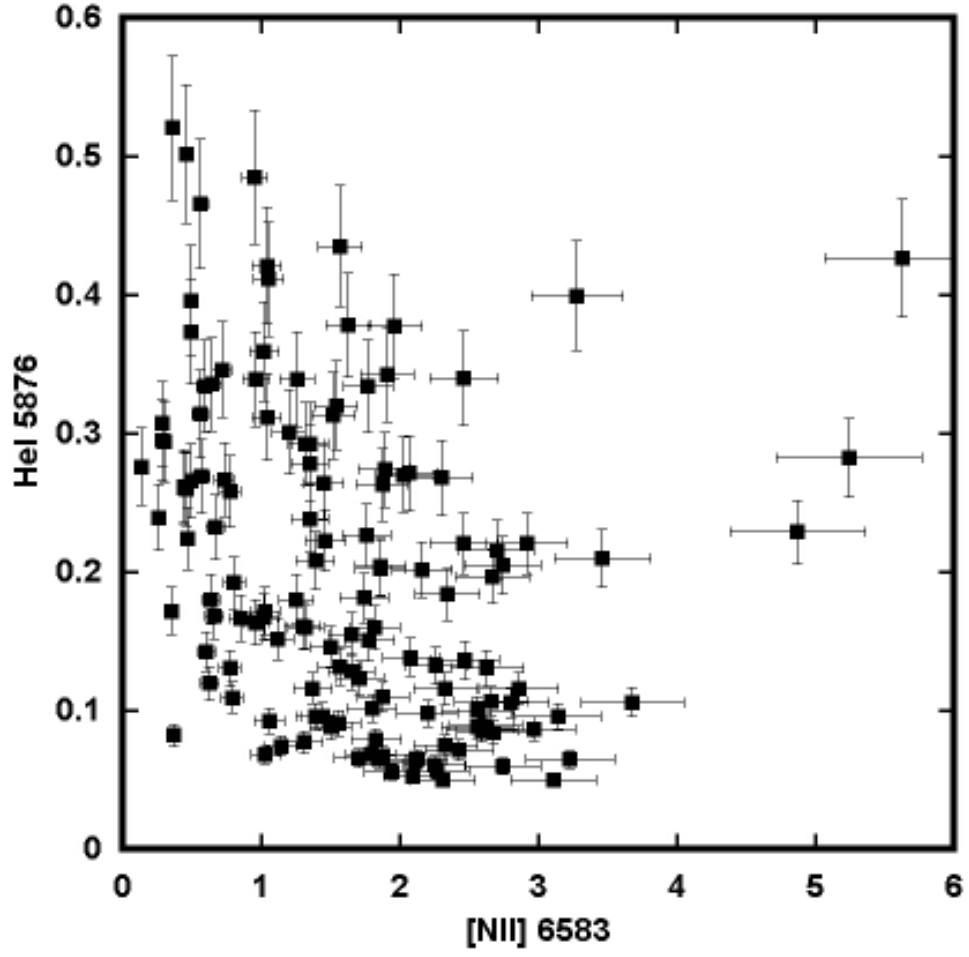


Fig. 12.— Correlation between  $H\alpha$ -normalized He I  $\lambda 5876$  and [N II]  $\lambda 6583$  line intensities. The error bars illustrate  $\pm 10\%$  uncertainties for both axes.